Climate Response of the Equatorial Pacific to Global Warming

PEDRO N. DINEZIO

Cooperative Institute for Marine and Atmospheric Studies, University of Miami, Miami, Florida

AMY C. CLEMENT

Rosenstiel School of Marine and Atmospheric Science, University of Miami, Miami, Florida

GABRIEL A. VECCHI

NOAA/Geophysical Fluid Dynamics Laboratory, Princeton, New Jersey

BRIAN J. SODEN AND BENJAMIN P. KIRTMAN

Rosenstiel School of Marine and Atmospheric Science, University of Miami, Miami, Florida

SANG-KI LEE

Cooperative Institute for Marine and Atmospheric Studies, University of Miami, Miami, Florida

(Manuscript received 12 December 2008, in final form 25 March 2009)

ABSTRACT

The climate response of the equatorial Pacific to increased greenhouse gases is investigated using numerical experiments from 11 climate models participating in the Intergovernmental Panel on Climate Change's Fourth Assessment Report. Multimodel mean climate responses to CO_2 doubling are identified and related to changes in the heat budget of the surface layer. Weaker ocean surface currents driven by a slowing down of the Walker circulation reduce ocean dynamical cooling throughout the equatorial Pacific. The combined anomalous ocean dynamical plus radiative heating from CO_2 is balanced by different processes in the western and eastern basins: Cloud cover feedbacks and evaporation balance the heating over the warm pool, while increased cooling by ocean vertical heat transport balances the warming over the cold tongue. This increased cooling by vertical ocean heat transport arises from increased near-surface thermal stratification, despite a reduction in vertical velocity. The stratification response is found to be a permanent feature of the equilibrium climate potentially linked to both thermodynamical and dynamical changes within the equatorial Pacific. Briefly stated, ocean dynamical changes act to reduce (enhance) the net heating in the east (west). This explains why the models simulate enhanced equatorial warming, rather than El Niño–like warming, in response to a weaker Walker circulation. To conclude, the implications for detecting these signals in the modern observational record are discussed.

1. Introduction

The response of the equatorial Pacific to increased greenhouse gases (GHGs) has been a matter of debate for over a decade. A range of atmosphere, ocean, and coupled processes has been invoked to explain why the zonal gradient of sea surface temperature (SST) should either increase or decrease as the earth warms (e.g., Knutson and Manabe 1995; Meehl and Washington 1996; Clement et al. 1996; Seager and Murtugudde 1997; Liu 1998; Meehl et al. 2000). While the current- and previous-generation coupled general circulation models (GCMs) project a weak reduction of the SST gradient into the twenty-first century (Collins et al. 2005; Meehl et al. 2007), the different reconstructions of SST observations of the twentieth century do not agree in the sign

Corresponding author address: Pedro N. DiNezio, 4600 Rickenbacker Causeway, Cooperative Institute for Marine and Atmospheric Studies, Rosenstiel School of Marine and Atmospheric Science, University of Miami, Miami, FL 33149.
E-mail: pdinezio@rsmas.miami.edu

DOI: 10.1175/2009JCLI2982.1

of the changes (Vecchi et al. 2008). Further, the observational analyses that suggest that the SST gradient has strengthened (Cane et al. 1997; Hansen et al. 2005, 2006; Karnauskas et al. 2009) would appear to be in contradiction with observational evidence for a weakening of tropical atmospheric circulation (Vecchi et al. 2006; Zhang and Song 2006; Bunge and Clarke 2009). These issues are unresolved, yet are of great importance because changes in the mean state of the equatorial Pacific could not only influence the behavior of El Niño–Southern Oscillation (ENSO; e.g., Jin 1996; Fedorov and Philander 2000, 2001; Timmermann et al. 1999), but also other regions through atmospheric teleconnections. For instance, trends in tropical cyclone intensity in the Atlantic basin (Vecchi and Soden 2007b; Wang and Lee 2008) and changes in the North American hydroclimate (Hoerling and Kumar 2003; Schubert 2004; Seager et al. 2005) have been linked with equatorial SSTs. Projecting the climate response of the equatorial Pacific into the twenty-first century is thus central for current efforts to understand future regional climate changes.

Prior studies have suggested roles for both the atmosphere and ocean in determining the response of the tropical Pacific to external forcing. For the ocean, changes in oceanic vertical heat transport have been proposed. For instance, an enhanced oceanic heat flux divergence could result from an increase in the surface thermal stratification associated with surface warming in the presence of unaltered climatological upwelling. As shown in relatively simple coupled models of the equatorial Pacific climate (Clement et al. 1996), this ''ocean dynamical thermostat'' produces colder temperatures in the eastern Pacific in response to a surface heating. In their model, the cooling response is the result of the Bjerknes feedback involving an increased zonal SST gradient and strengthened atmospheric circulation.

Mechanisms involving atmospheric processes only have also been suggested. A weakening of the tropical atmospheric circulation in response to increased GHGs has been found to be both a robust feature across an ensemble of 22 state-of-the-art climate models, and linked with a reduction of the equatorial east–west SST gradient (Vecchi and Soden 2007a). According to this study, a slowing down of the simulated Walker circulation results from global thermodynamic constraints on the response of the hydrologic cycle to global warming (GW) (Held and Soden 2006). Increased dry static stability in the tropics can also contribute to the reduction of the tropical circulation (Knutson and Manabe 1995). Simulations of the climate of the twentieth century are consistent with observed long-term trends, showing a reduction of the east–west sea level pressure (SLP) difference during 1861–2000 (Vecchi et al. 2006). This weakening of the tropical atmospheric circulation has been invoked to explain the weakening in the zonal SST gradient simulated by the GCM experiment performed for the Intergovernmental Panel on Climate Change (IPCC) Fourth Assessment Report (AR4; e.g., Meehl et al. 2007). Evaporation and cloud feedbacks have also been proposed to explain a reduction in the SST gradient. For instance, given a uniform surface warming, the east–west differential in evaporative damping can produce an enhanced SST response in the cold tongue (Wallace 1992; Knutson and Manabe 1995). Similarly, cloud feedbacks associated with shortwave (SW) surface fluxes have been proposed. In this case, the zonal asymmetry in SST response arises from different cloud regimes across the basin, leading to a negative (stabilizing) cloud albedo feedback over the warm pool (Ramanathan and Collins 1991; Meehl and Washington 1996; Meehl et al. 2000) and a positive (amplifying) cloud cover feedback over the cold tongue (Klein and Hartmann 1993).

All of these processes are included in current state-of-the-art coupled climate models, yet the answer from those models with respect to the zonal SST gradient remains unclear. The majority of the current- and previous generation models project a mean El Niño–like response in the tropical Pacific, with the central and eastern equatorial Pacific SST warming more than the western equatorial Pacific (Cubasch et al. 2001; Meehl et al. 2007). However, some model intercomparison analyses suggest that no change in the zonal SST gradient is more likely than an El Niño–like change (Collins et al. 2005; Liu et al. 2005).

In this study we analyze the response of the equatorial Pacific to GW using a coordinated set of 11 climate model experiments. Following Vecchi et al. (2008), we hypothesize that the SST changes in response to increased GHGs result from the superposition of the ocean response to both a weakening of the Walker circulation and an increase in thermal stratification (ocean dynamical thermostat). The details of this interaction and the role of other potentially important processes, such as clouds, are explored through a heat budget analysis of the models' output. The organization of this paper is as follows: In section 2 we describe the models and global warming experiments considered. Section 3 presents the spatial signature of the SST response we seek to understand. The changes in surface heat fluxes and clouds are analyzed in sections 4 and 5. In sections 6 to 8 we link multimodel mean changes in the atmospheric circulation and thermal structure of the upper ocean with changes in the heat budget of the surface layer. We conclude with a discussion of the atmosphere, ocean, and coupled responses that determine the simulated SST in the warm pool and the cold tongue, and possible ways of detecting these mechanisms in the real world.

TABLE 1. IPCC AR4/CMIP3 from which data for the experiments used in this analysis (1pctto2x and picntrl) are available in the WCRP CMIP3 dataset.

Model	Model resolution		Reference
	Ocean	Atmosphere	
Geophysical Fluid Dynamics Laboratory (GFDL) Climate Model version 2.0 (CM2.0)	1° × 1° (1/3°) L50	2.5° × 2° L24	Delworth et al. (2006)
GFDL Climate Model version 2.1 (CM2.1)	1° × 1° (1/3°) L50	2.5° × 2° L24	Delworth et al. (2006)
Meteorological Research Institute (MRI) Coupled General Circulation Model, version 2.3.2a (CGCM2.3.2a)	2.5° × 0.5° L23	T42 L30	Yukimoto and Noda (2002)
Center for Climate System Research/National Institute for Environmental Studies/Frontier Research Center for Global Change Model for Interdisciplinary Research on Climate 3.2, medium-resolution version [MIROC3.2(medres)]	1.4° × 0.5° L43	T42 L20	Hasumi and Emori (2004)
Institute of Numerical Mathematics Coupled Model, version 3.0 (INM-CM3.0)	2.5° × 2° L33	5° × 4° L21	Volodin and Diansky (2004)
National Center for Atmospheric Research (NCAR) Community Climate System Model, version 3 (CCSM3.0)	1.1° × 1.1° (0.27°) L40	T85 L26	Collins et al. (2006)
Canadian Centre for Climate Modelling and Analysis (CCCma) CGCM, version 3.1 (CGCM3.1)	1.85° × 1.85° L29	T47 L31	Flato and Boer (2001)
Centre National de Recherches Météorologiques Coupled Global Climate Model, version 3 (CNRM-CM3)	2° × 0.5° L31	T63 L45	Salas-Mélia et al. (2005)
European Centre Hamburg Model, version 5 (ECHAM5)/Max Planck Institute Ocean Model (MPI-OM)	1.5° × 0.5° L40	T63 L31	Marsland et al. (2003)
Institute of Atmospheric Physics (IAP) Flexible Global Ocean–Atmosphere–Land System Model gridpoint version 1.0 (FGOALS-g1.0)	1° × 1° L33	T42 L26	Yu et al. (2004)
L'Institut Pierre-Simon Laplace Coupled Model, version 4 (IPSL CM4)	2° × 0.5° L31	2.5° × 3.75° L19	Goosse and Fichefet (1999)

2. $2 \times CO_2$ climate experiments

Climate change simulations from 11 coupled GCMs integrated with CO_2-doubling ($2 \times CO_2$) emission scenarios are analyzed and compared with control simulations forced solely with preindustrial CO_2 concentrations. These numerical simulations are part of the World Climate Research Programme's (WCRP's) Coupled Model Intercomparison Project phase 3 (CMIP3) multimodel dataset and were performed for the IPCC's AR4. Eight out of the 11 models analyzed here (Table 1, all model acronyms defined) do not perform flux correction. MRI CGCM2.3.2a performs flux adjustment for heat, water, and momentum; CCCma CGCM3.1 performs flux adjustment for heat and water; and INM-CM3.0 performs flux adjustment for water. Eleven models out of 22 submitted to CMIP3 are included in the ensemble because the remaining models do not include ocean temperature and velocity variables for the preindustrial control (picntrl) or for the 1% yr^{-1} CO_2 increase to doubling (1pctto2x) experiments.

For each model, the CO_2-doubling experiment starts from the respective control simulation, increasing CO_2 concentrations at a rate of 1% yr^{-1}, from 280 ppm until doubling (560 ppm) on year 71. These experiments have been run for at least 150 additional years with constant $2 \times CO_2$ concentrations. No other radiative forcing is considered in both the picntrl and 1pctto2x experiments. For MRI CGCM2.3.2 the present-day experiment (pdcntrl) is used as the control for the 1pctto2x experiment according to the documentation of this model. Only one experiment from each model (typically run 1 in the CMIP3 dataset) is included in the 11-model ensemble. Run 3 of the 1pctto2x experiment is used for ECHAM5/MPI-OM and run 2 of the picntrl experiment is used for NCAR CCSM3 because these are the only runs with complete ocean data.

Our heat budget analysis is restricted to the tropics where the climate reaches equilibrium faster, compared with high latitudes, where ice–albedo feedbacks are important. For instance, 50 yr after CO_2 concentrations are doubled, the tropical-mean surface temperature trend is less than 0.3 K $(100\ yr)^{-1}$ in all models, with the exception of IPSL CM4 with a 0.4 K $(100\ yr)^{-1}$ trend. Some of the models show a transient cooling trend of less than 0.2 K during the first 100 yr of the picntrl

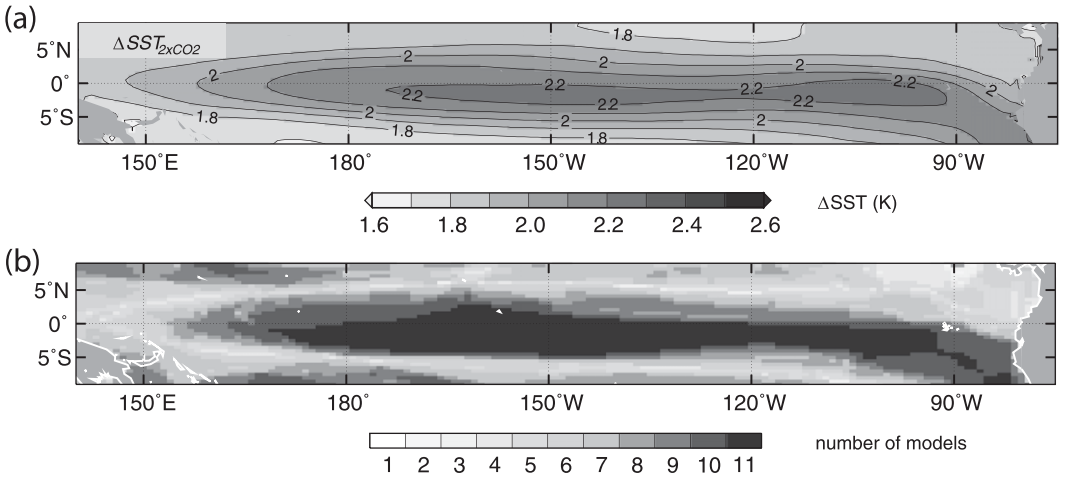

FIG. 1. (a) Multimodel ensemble-mean SST response to $2 \times CO_2$. Here and in succeeding figures the $2 \times CO_2$ response in each model is computed as the difference between 100-yr climatologies of the near-equilibrium $2 \times CO_2$ (1pctto2x) and control (picntrl) experiments. The ensemble-mean tropical sensitivity, defined as the mean surface temperature change between 30°S and 30°N both over land and ocean, is 2.1 K. (b) Number of models simulating a SST response larger than each model's tropical sensitivity.

experiment. INM-CM3.0 and NCAR CCSM3.0 have cooling trends over the entire picntrl experiment of about 0.1 $(300\ \text{yr})^{-1}$ and 0.3 $(500\ \text{yr})^{-1}$, respectively. These trends imply heat storage rates in the upper 100 m of the ocean that are no larger than 0.1 W m^{-2}, which is one order of magnitude smaller than the $2 \times CO_2$ changes in net surface heat flux (Fig. 2), and therefore unlikely to influence the conclusions of this study. Thus, near-equilibrium climates are computed using monthly fields from year 121 to year 220 of the 1pctto2x experiments and years 1–100 of the picntrl experiments. The near-equilibrium $2 \times CO_2$ climate is computed over 80 yr for GFDL CM2.1 and over 30 yr for ECHAM5/MPI-OM because only 200 and 150 yr of ocean data are available, respectively.

Throughout this study we focus on those aspects of the climate response that appear in the multimodel mean. To provide an indication of how robust these signals are across the different models, we also include for certain variables the number of models having the same sign change (e.g., Fig. 2b). This robustness ''estimator'' does not provide information about how close the models' responses are from the ensemble mean, and thus is unable to detect outliers. However, it remains useful in our study, because much of the debate on the climate response of the equatorial Pacific to GW has been on whether some processes, such as the ocean dynamical thermostat or cloud feedbacks, are represented by GCMs with the appropriate sign. In addition, we analyzed the response by each individual model to avoid making invalid conclusions from the multimodel mean.

3. Sea surface temperature response

The simulated near-equilibrium $2 \times CO_2$ SST response shows enhanced warming concentrated in the equatorial Pacific in all models (Fig. 1a), with SSTs increasing by about the magnitude of tropical sensitivity and extending west of the date line (Fig. 1b). This enhanced equatorial warming (EEW) has been linked to enhanced evaporative cooling in the subtropics with respect to the equator (Liu et al. 2005). Changes in the east–west contrast, both positive and negative, are superposed on this multimodel EEW. The majority of models, nonetheless, show a very subtle weakening of the east–west contrast of less than 0.1 K between Niño-3 and Niño-4 regions, consistent with the results of Collins et al. (2005). The spatial signature of the SST changes could be described as being El Niño like; however, the equatorial warming extends farther west than the SST anomalies associated with a typical El Niño event. Moreover, the anomalous zonal SST gradient in response to $2 \times CO_2$ is much weaker and is confined to the west of the date line. Note that the *simulated* El Niño events show SST anomalies that also extend west from the date line compared with *real* events (not shown). Only three models, MRI CGCM2.3.2, ECHAM5/MPI-OM and CCCma CGCM3.1, show unambiguous El Niño–like SST responses, with much larger anomalous SST gradients in the central Pacific. NCAR CCSM3.0 simulates a strengthening of the SST gradient, without a clear La Niña–like pattern. The remaining models show SST signatures with no clear indication of equatorial-wide changes in gradient.

TABLE 2. Feedbacks operative in the equatorial Pacific proposed by previous studies. The different feedbacks are organized according to their influence on the zonal SST gradient during the response to Global Warming.

Feedback/process	Region	Type	Ocean dynamics?	Reference
Feedbacks decreasing the zonal SST gradient				
SST–Q_{LH}	Basin wide	Negative	No	Wallace (1992); Knutson and Manabe (1995)
SST–Q_{SW}	Warm pool	Negative	No	Ramanathan and Collins (1991); Meehl et al. (2000)
	Cold tongue	Positive	No	Klein and Hartmann (1993)
Weaker Walker + Bjerknes	Basin wide	Positive	No	Vecchi and Soden (2007a)
	Basin wide		Yes	Bjerknes (1969); Dijkstra and Neelin (1995)
Feedbacks increasing the zonal SST gradient				
Ocean thermostat	Cold tongue	Negative	Yes	Clement et al. (1996)

The El Niño–like response is typically attributed to the weakening of the atmospheric circulation (Vecchi and Soden 2007a; Meehl et al. 2007), reducing ocean dynamical cooling in the east Pacific, which, along with and other atmospheric feedbacks (Knutson and Manabe 1995; Meehl and Washington 1996), would result in a larger SST response in the east. However, not all the models analyzed here simulate El Niño–like SST changes despite a robust weakening of the Walker circulation (Vecchi and Soden 2007a,b). A role for the ocean dynamical changes has been suggested from analysis of the CMIP3 models and could balance the effect of weaker winds (Vecchi et al. 2008). This study showed that fully coupled models, which allow for changes in ocean heat flux divergence, simulate a smaller SST increase in the equatorial cold tongue. In contrast, models where the ocean heat flux divergence is prescribed show a clear El Niño–like response. This apparent cooling resulting from ocean dynamics could result from changes in thermal stratification (Clement et al. 1996), even if upwelling is reduced due to weaker winds. An important role for ocean dynamics is expected in the cold tongue, where vertical heat transport dominates the heat budget of the surface layer controlling the SSTs (e.g., Wyrtki 1981; Seager et al. 1988). The westward extent of the warming suggests that changes in zonal advection could also play a role at the edge of the warm pool. Throughout the rest of this study we analyze the changes in the heat balance of the surface layer in order to elucidate the role of ocean dynamics in the simulated climate response.

4. Changes in surface fluxes

As the earth's surface warms, acting to equilibrate the $2 \times CO_2$ radiative perturbation at the top of the atmosphere (TOA), radiative feedbacks, such as the water vapor feedback or cloud feedbacks, amplify the surface response (e.g., Soden and Held 2006). A complex interplay of radiative and surface feedbacks represented in the temperature equation of the surface layer determines the SST response. Different feedbacks have been proposed to operate in the GW response of the equatorial Pacific. Table 2 summarizes their influence on the zonal SST gradient in the GW response. These feedbacks operate through the dependence of the surface fluxes on SST, through large-scale coupled ocean–atmosphere processes, such as the climatological Bjerknes feedbacks (Dijkstra and Neelin 1995), or through changes in ocean heat transport, such as the ''ocean dynamical thermostat'' (Clement et al. 1996).

A change in net surface heat fluxes is possible in the equilibrium $2 \times CO_2$ climate, which is ultimately balanced by changes in oceanic heat flux divergence. This balance is determined by the interplay of the different atmospheric and coupled feedbacks in the SST equation (Table 2). The ensemble-mean change in net surface heat flux ΔQ_{net} shows a marked zonal asymmetry, with cooling over the warm pool and heating over the cold tongue (Fig. 2a). This response is simulated by all 11 models (Fig. 2b), with the exception of INM-CM3.0 and NCAR CCSM3, in which the positive ΔQ_{net} in the west is negligible. This anomalous heat flux has to be in equilibrium with changes in oceanic heat flux convergence–divergence because the climate system is nearly in equilibrium and the changes in heat storage rate are negligible. In both the control and $2 \times CO_2$ climates and in the earth's climate, the oceanic heat flux divergence is positive (cooling) throughout the equatorial Pacific; therefore, these changes in net surface heat flux represent a reduction (increase) in ocean dynamical cooling in the west (east).

This zonal asymmetry in the response does not result from the anomalous heating resulting from changes in either clear-sky radiation $\Delta Q_{clear\text{-}sky}$ or sensible heat fluxes ΔQ_{SH}, which show uniform multimodel responses of about 7 and 2 W m^{-2}, respectively (not shown). The clear-sky radiation response represents the dominant heating term in the heat budget changes and results from an increase in downward longwave (LW) clear-sky radiation, consistent with increased atmospheric emission

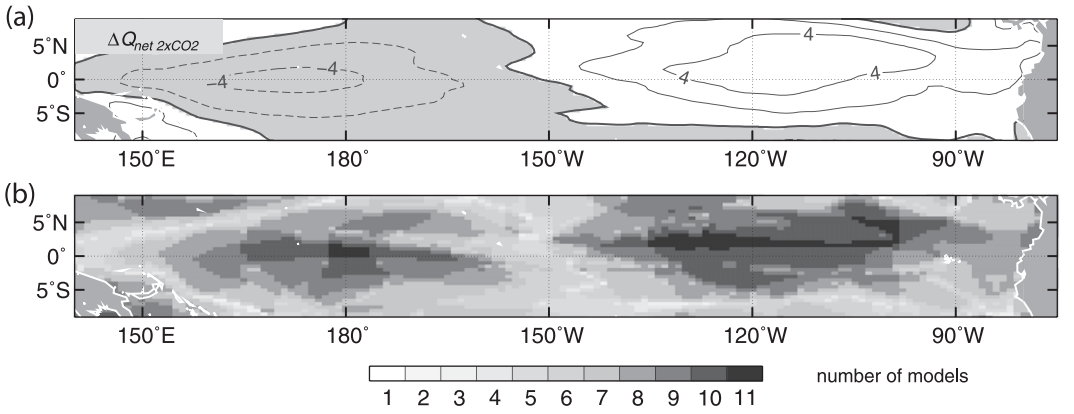

FIG. 2. (a) Multimodel ensemble-mean change in net surface heat flux, ΔQ_{net}, in response to $2 \times CO_2$. The contour interval is 2 W m^{-2}. Grayed regions and dashed contours indicate negative values. Positive values are into the ocean. (b) Number of models simulating a ΔQ_{net} with the same sign as the 11-model ensemble-mean response.

associated with the water vapor and lapse-rate feedbacks, which is partially balanced by increased upward LW radiation, consistent with increased surface emission associated with the Planck feedback. A reduction in clear-sky SW surface radiation also contributes to the Planck feedback, reducing the net clear-sky radiation, and could be related to absorption by water vapor (Takahashi 2009).

The east–west asymmetry in ΔQ_{net} results from the responses in both SW radiation ΔQ_{SW} (Fig. 3a) and latent heat fluxes ΔQ_{LH} (Fig. 3b). In the warm pool, their combined effect leads to cooling that exceeds the radiative plus sensible heating, and results in net cooling (Fig. 2). On the contrary, both ΔQ_{SW} and ΔQ_{LH} are negligible in the cold tongue, leaving ocean dynamical changes to balance the increase in radiative plus sensible heat fluxes. Although ΔQ_{LH} is negligible in the cold tongue, this response is likely to result from the cancellation between reduced evaporation resulting from reduced wind speed and an increased evaporation associated with larger SSTs. However, the spatial pattern of ΔQ_{LH} (Fig. 3b) does not suggest a dominant role for the nonlinearity of the humidity–SST relationship, as proposed by Knutson and Manabe (1995).

5. Cloud changes

East–west asymmetries in ΔQ_{net} have been argued to arise from surface radiation changes associated with the different cloud regimes across the basin (Meehl and Washington 1996; Meehl et al. 2000). The multimodel changes in surface radiation resulting from clouds (ΔQ_{cloud}, Fig. 4a) shows the same signature as ΔQ_{SW} (Fig. 3a),

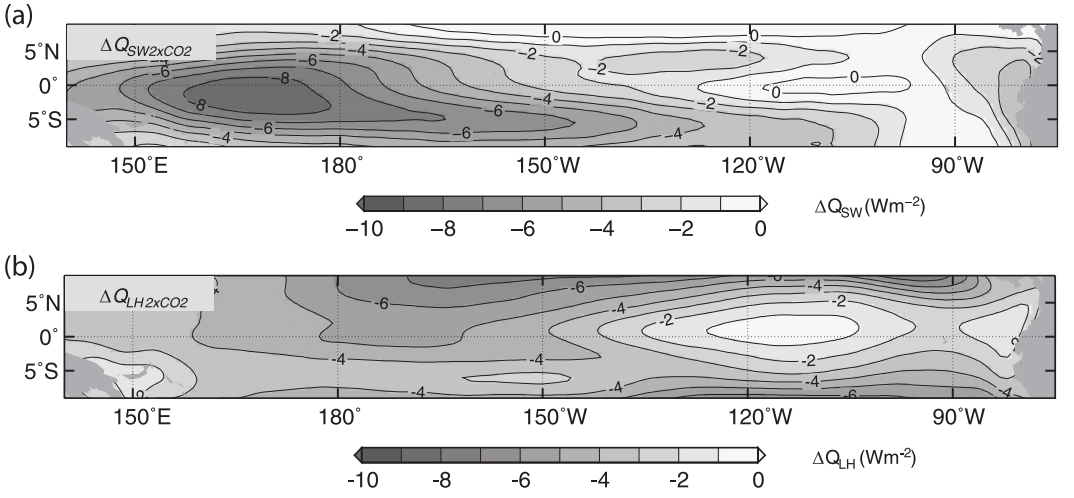

FIG. 3. Multimodel ensemble-mean changes in (a) surface shortwave radiation and (b) latent heat fluxes in response to $2 \times CO_2$. In both panels positive values are into the ocean.

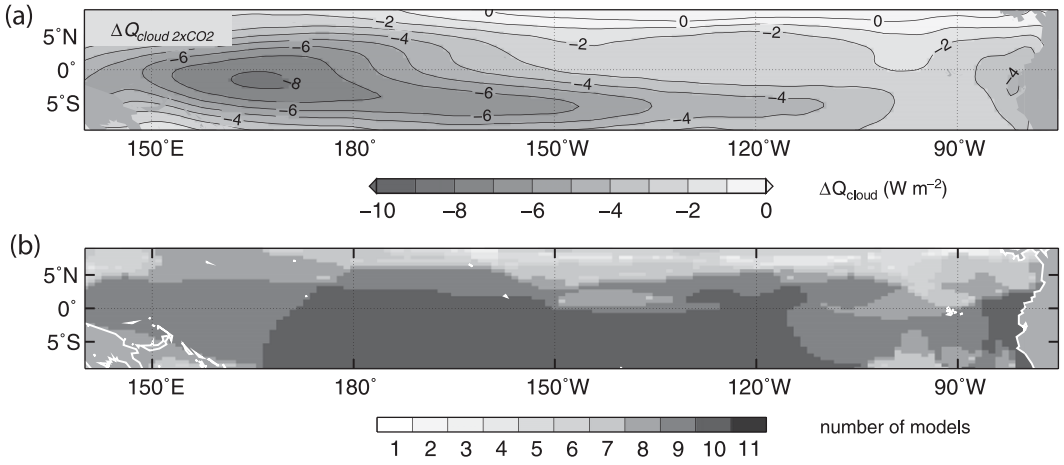

FIG. 4. (a) Multimodel ensemble-mean change in surface cloud radiation in response to 2 × CO_2. The changes in surface radiation resulting from clouds, ΔQ_{cloud}, include changes in SW and LW radiation. Positive values are into the ocean. (b) Number of models simulating ΔQ_{cloud} with the same sign as the 10-model ensemble-mean response. FGOALS-g1.0 was not included because of a lack of data in the CMIP3 database.

indicating that the changes in SW radiation are driven by cloud changes. The largest response is simulated in the warm pool, where high clouds are the dominant cloud regime. Changes in cloud albedo (Fig. 5) suggest an increase in the reflectivity of warm pool high clouds, simulated by all models. While this is consistent with a negative cloud–albedo feedback (Ramanathan and Collins 1991; Meehl et al. 2000), the changes are collocated with increases in cloud fraction (Fig. 6) that could be driving the reduction in SW radiation reaching the ocean surface. These cloud changes could be interpreted as an El Niño–like shift in the cloud climatology; however, the westward increase in cloudiness is not accompanied by a reduction over Indonesia.

In the cold tongue, the surface heating resulting from ΔQ_{SW} is not robust. Only four models [MIROC3.2-(medres), NCAR CCSM3, IPSL CM4, and MRI CGCM2.3.2] simulate positive ΔQ_{SW}, consistent with a positive cloud cover feedback (Klein and Hartmann 1993). Moreover, this response is cancelled by a negative LW response leading to negligible cooling (Fig. 4). Regardless of this strong positive feedback, only MRI CGCM2.3.2 simulates a clear El Niño–like SST change. It should be noted that the stabilizing effect of high clouds has been disputed in several papers (Wallace 1992; Hartmann and Michelsen 1993; Pierrehumbert 1995). Those studies showed that because the TOA SW and LW forcing of these clouds cancel, they cannot

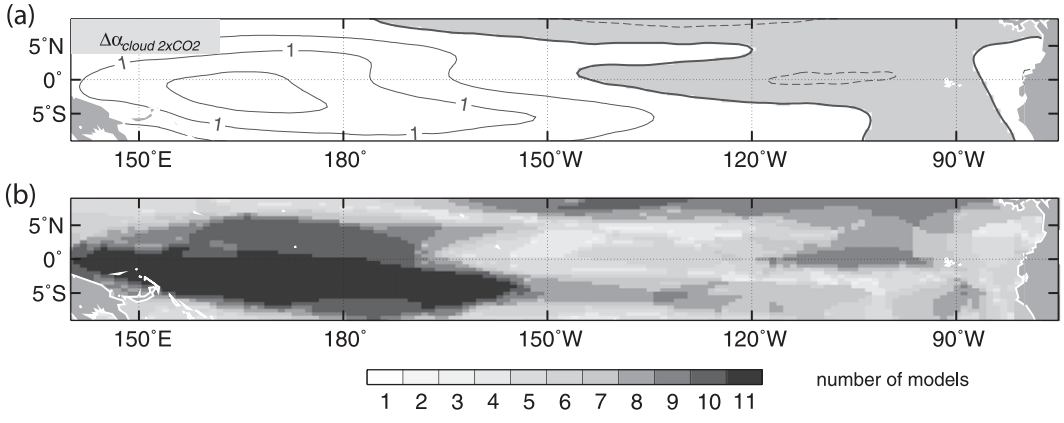

FIG. 5. (a) Multimodel ensemble-mean change in cloud albedo in response to 2 × CO_2. The contour interval is 0.5%. Grayed regions and dashed contours indicate a decrease in cloud albedo. (b) Number of models simulating a cloud albedo change with the same sign as the 11-model ensemble-mean response.

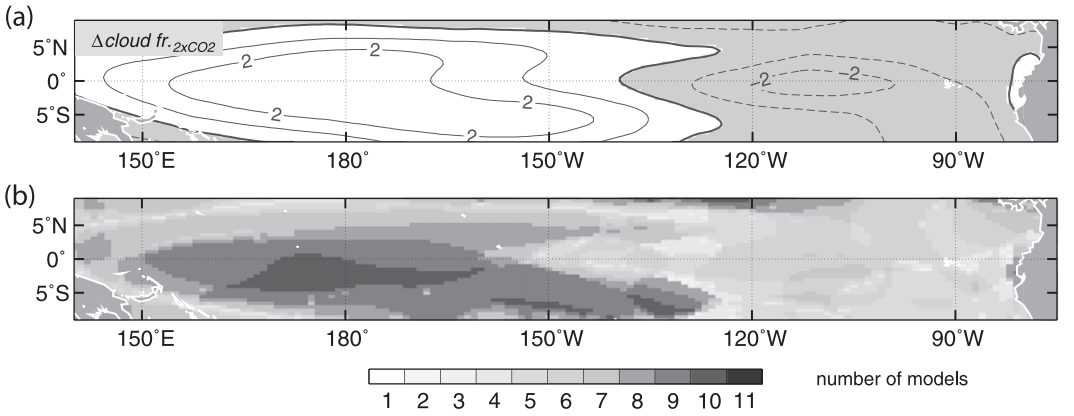

FIG. 6. (a) Multimodel ensemble-mean change in column-integrated cloud cover in response to 2 × CO_2. The contour interval is 1%. Grayed regions and dashed contours indicate a decrease in cloud cover. (b) Number of models simulating a cloud cover change with the same sign as the 11-model ensemble-mean response.

affect the planetary energy budget. In this ensemble of models, the cloud response shows some degree of cancellation. Nonetheless, the cloud response simulated by the GCMs is consistent with the studies indicating that high clouds can have an impact on the spatial distribution of surface SW radiation (Collins et al. 1996; Sobel 2003), if not the tropical-mean radiation budget.

6. Changes in the atmospheric circulation

The multimodel mean atmospheric circulation shows reductions in the zonal SLP pressure gradient across models (Fig. 7a). A pattern of weakened zonal wind stress is also simulated over a meridionally narrow band. Part of the weakening of the atmospheric circulation may be driven by the SST changes; however, the SST response (Fig. 1a) shows little change in the zonal SST gradient that could drive anomalous atmospheric circulation. A weakening of the Walker circulation could also result from processes external to the equatorial Pacific climate (Held and Soden 2006; Vecchi and Soden 2007a). According to these studies, a slowing of the atmospheric overturning circulation results from the different responses of global-mean precipitation and atmospheric humidity to GW. As the earth warms, near-surface humidity increases by 7% K^{-1} (following the Clausius–Clapeyron relationship); however, the strength of the simulated hydrological cycle increases at a slower rate of 2% K^{-1}. This differential in sensitivities represents a robust constraint for the global-scale tropical circulation, because mass fluxes in precipitating convective towers have to reduce by 5% K^{-1}, weakening the large-scale Walker circulation as a result. Evidence for this mechanism has been

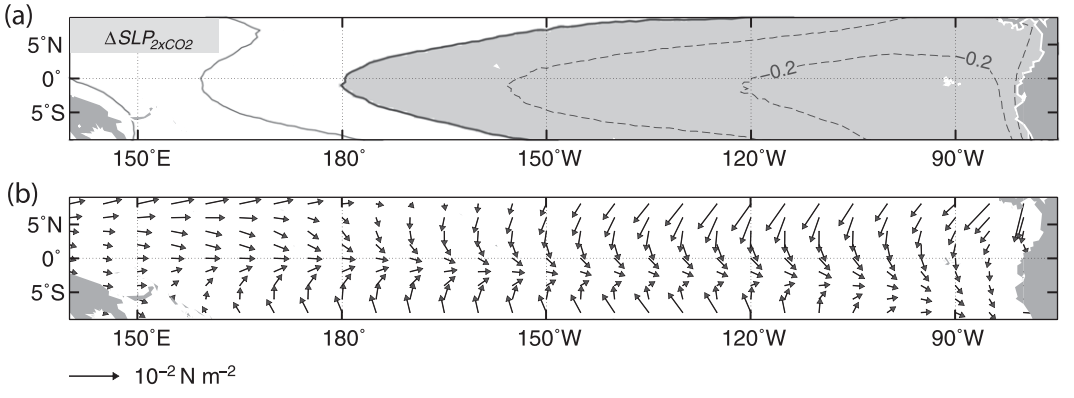

FIG. 7. Multimodel ensemble-mean change in (a) SLP and (b) surface wind stress in response to 2 × CO_2. The contour interval is 0.5 hPa. Grayed regions and dashed contours indicate negative values. Note that the mean SLP is larger in the east as in the west, thus the simulated pattern corresponds to a reduced zonal gradient.

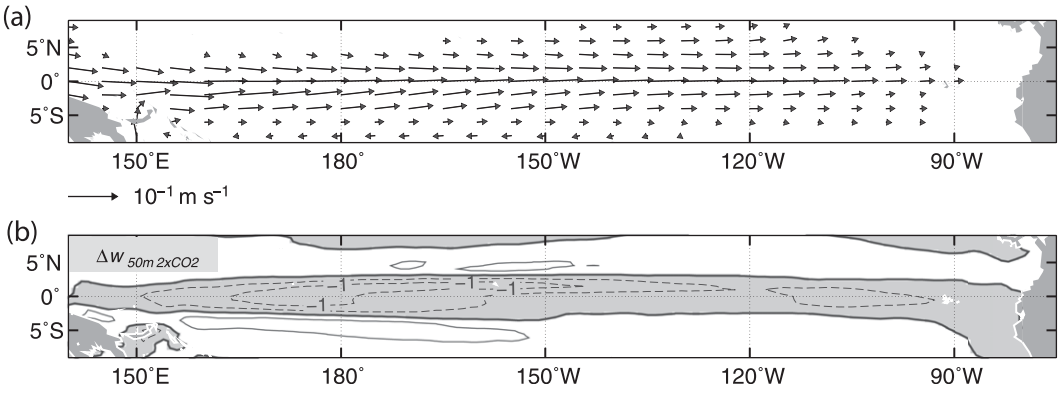

FIG. 8. Multimodel ensemble-mean changes in ocean (a) surface currents and (b) vertical velocity in response to $2 \times CO_2$. The surface currents are averaged over the top 50-m layers of the models. The vertical velocity (positive upward) is at a depth of 50 m. The contour interval is 0.5×10^{-1} m day^{-1}. Grayed regions and dashed contours indicate negative values.

provided through an analysis of robust responses of convective mass fluxes and precipitation across a larger ensemble of IPCC AR4/CMIP3 models, including those analyzed here (Vecchi and Soden 2007a).

7. Ocean dynamical response to a weakening of the Walker circulation

Theory, numerical models, and observations indicate that the response of the equatorial ocean to a relaxation of the trade wind winds consists of 1) a weakening of the equatorial surface currents, 2) a reduction in Ekman divergence and weakened equatorial upwelling, 3) a reduction of the east–west thermocline tilt, and 4) a shallower zonal-mean thermocline depth or a discharge in equatorial heat content in response to the curl of the wind (e.g., Cane 1979; Philander 1981; McPhaden 1993). In the GW response, thermodynamical changes, such as stratification changes associated with the surface warming (e.g., Gnanadesikan et al. 2007) or the interaction with the subtropics through the large-scale shallow meridional overturning (e.g., Seager and Murtugudde 1997; McPhaden and Zhang 2002), may also be superimposed on the dynamical thermocline responses (i.e., 3 and 4).

The multimodel ocean response analyzed here is consistent with an ocean dynamical adjustment to weaker winds, showing a multimodel weakening of the equatorial currents (Fig. 8a) and reduced upwelling (Fig. 8b). An analysis of the changes in ocean thermal structure (Fig. 9b) suggests both dynamical and thermodynamical responses in the thermocline. The ensemble of models simulates the equatorial thermal structure in qualitative agreement with observations (Fig. 9a) with isotherms deepening toward the west and with the 20°C isotherm located in the layer of large temperature gradients. A basin-wide anomalous warming is simulated throughout the upper 100 m of the ocean in response to $2 \times CO_2$ (Fig. 9b), with an anomalous stratification at the base of the mixed layer. The absence of subsurface warming at depths of about 200 m in the western Pacific suggests a dynamical response in addition to the thermodynamical response to the surface warming. This reduced warming could result from a relaxed, and thus shallow, thermocline bringing deeper and colder waters upward.

The thermocline response to $2 \times CO_2$ is clearly identified in the changes in vertical temperature gradient $\partial T/\partial z$ (Fig. 10b). The multimodel ensemble-mean equatorial thermocline is identified as the region of the largest values of $\partial T/\partial z$ in the control experiments (Fig. 10a). The $2 \times CO_2$ changes (Fig. 10b) show a uniform pattern of increased and decreased values of $\partial T/\partial z$ above and below the location of the maximum $\partial T/\partial z$ in the control climate. This response indicates a basinwide shoaling of the thermocline in the equatorial Pacific, consistent with a discharge of equatorial heat content in response to the changes in curl of the wind. Because the thermocline shoals even in the eastern Pacific, the subsurface warming simulated in the east (Fig. 9b) is likely to be related with increased ocean heat transport by upwelling and vertical mixing instead of a deepening of the thermocline.

A sharpening of the thermocline is also suggested from the $\partial T/\partial z$ changes, because the near-surface increase in $\partial T/\partial z$ is larger that the decrease below the thermocline. This anomalous near-surface thermal stratification could be related to a thermodynamic response to the surface warming (mechanism 5 above). Clearly, the GW response of the thermal structure of the equatorial ocean results from both thermodynamic and dynamic processes.

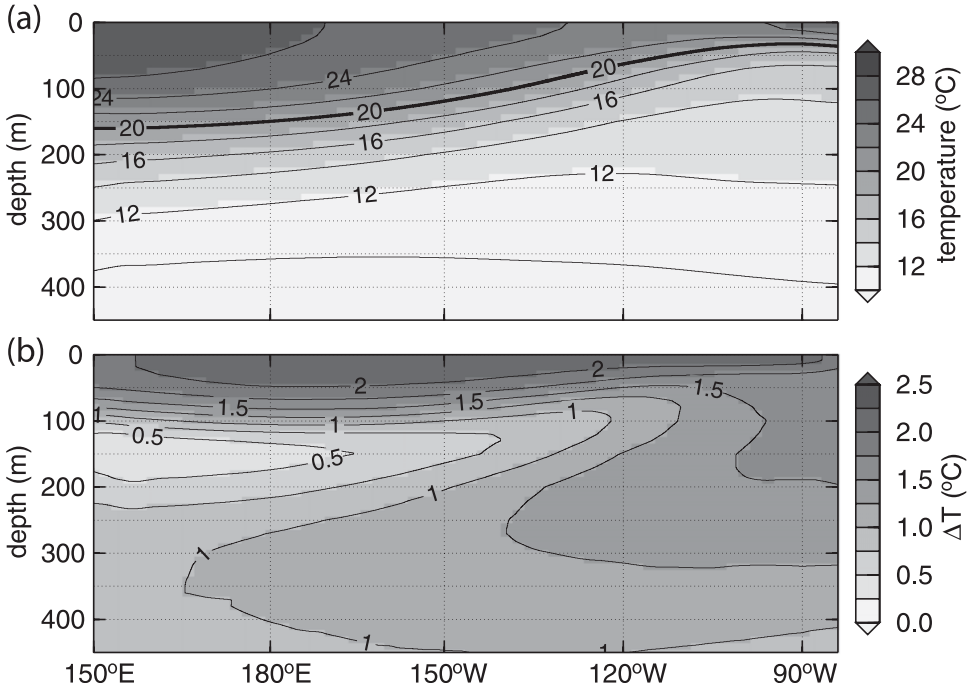

FIG. 9. (a) Multimodel ensemble-mean thermal structure at the equator in the control experiments and (b) response to 2 × CO_2. The equatorial sections are averaged over the 2°S and 2°N latitude band.

A comprehensive attribution of the changes in the equatorial thermocline and the effect on the surface stratification will be the subject of a future study. In this study we will focus on how these changes in near-surface stratification and currents influence the heat budget of surface layer through changes in ocean heat transport.

8. Changes in ocean heat transport

In this section we explore the changes in oceanic heat flux divergence by estimating the vertically integrated zonal (Q_u), meridional (Q_v), and vertical (Q_w) ocean dynamical heating contributions as

$$Q_u = -\rho_0 c_p \int_{-H}^{0} u \frac{\partial T}{\partial x}\, dz$$
$$Q_v = -\rho_0 c_p \int_{-H}^{0} v \frac{\partial T}{\partial y}\, dz \qquad (1)$$
$$Q_w = -\rho_0 c_p \int_{-H}^{0} w \frac{\partial T}{\partial z}\, dz,$$

where we chose $H = 75$ m to estimate the heat budget of the surface layer. Qualitatively, the balance of processes will not depend on the depth of integration for the temperature advection terms (1). More details on how the heat budget of the surface layer can be recomputed from model output and the sensitivity of the results to the depth of integration are given in the appendix.

Changes in zonal heat transport (ΔQ_u; Fig. 11a) are found in a narrow equatorial band coinciding with the region of weakened zonal currents (Fig. 8a). Most of the response results from changes in zonal currents rather than from anomalous zonal temperature gradients. This response is simulated by all models, with the exception of INM-CM3.0. In this model, the absence of a strong zonal SST gradient, due to a cold tongue extending throughout the entire basin, results in negligible changes despite weaker zonal currents. The change in meridional advection ΔQ_v shows off-equatorial maxima (Fig. 11b) resulting from anomalous meridional temperature gradients associated with the enhanced equatorial SST response (Fig. 1a), rather that from reduced Ekman divergence in response to the weaker winds (not shown). The lateral (zonal and meridional) advection terms are important cooling terms in the heat budget of the surface layer outside of the cold tongue, where vertical processes dominate. Both changes in zonal and meridional heat advection represent ocean dynamical heating (Fig. 12) extending over most of the equatorial Pacific.

Different ocean processes drive the changes in zonal advection ΔQ_u along the equator (Fig. 11a). Weakened surface currents drive anomalous ocean dynamical heating in the warm pool, as discussed above. However, in the cold tongue, the response results from a shallower

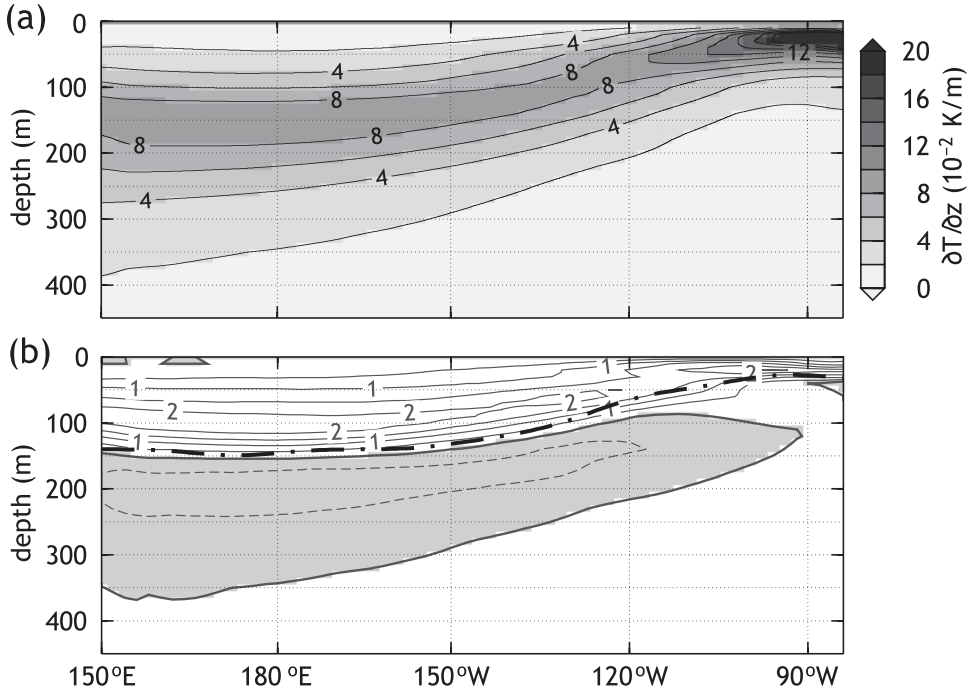

FIG. 10. (a) Multimodel ensemble-mean vertical temperature gradient at the equator in the control experiments and (b) response to 2 × CO_2. The equatorial sections are averaged over the 2°S and 2°N latitude band. In (b) the dashed–dotted line indicates the location of the maximum vertical temperature gradient in the control run. The contour interval is 0.5×10^{-2} K m^{-1}. Grayed regions and dashed contours indicate negative values.

equatorial undercurrent (EUC), which outcrops farther west, increasing the advection of warm waters from the warm pool into the cold tongue. In the warm pool the changes in vertical advection are expected to be negligible and the anomalous ocean dynamical heating resulting from horizontal currents is likely to be balanced by the changes in net surface fluxes. However, in the cold tongue the changes in surface fluxes and the lateral heat transport are all positive and have to be balanced by changes in vertical heat transport.

Multimodel changes in vertical advection ΔQ_w, with up to -20 W m^{-2} values, are simulated in the central and east Pacific, centered at the equator (Fig. 13). This response represents an enhancement of the ocean dynamical cooling resulting from upwelling in the cold tongue, which is O(100 W m^{-2}) in the annual mean. Two different types of processes can give rise to such enhanced cooling: an increase in upwelling or an increase in the stratification. Only an increase in ocean thermal stratification can drive this response because upwelling is

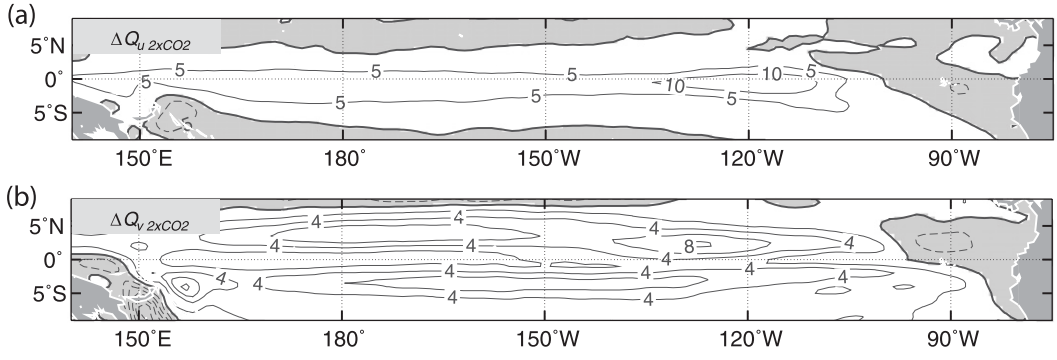

FIG. 11. Multimodel ensemble-mean change in (a) zonal heat transport and (b) meridional heat transport in response to 2 × CO_2. Positive values imply heating of the ocean surface layer. The contour interval is 5 W m^{-2}. Grayed regions and dashed contours indicate negative values.

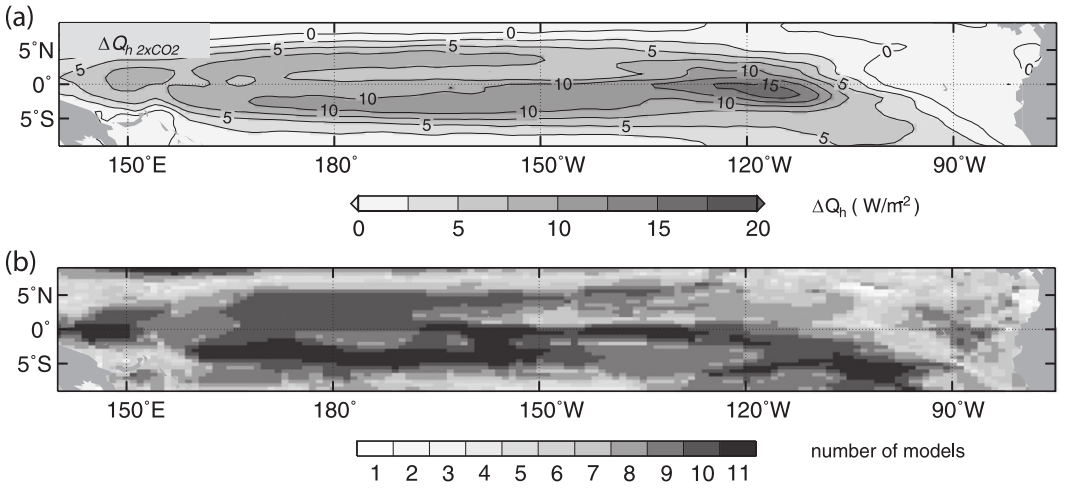

FIG. 12. Multimodel ensemble-mean change in lateral (zonal plus meridional) heat transport in response to $2 \times CO_2$. Positive values imply heating of the ocean surface layer. (b) Number of models simulating a heat transport change with the same sign as the 11-model ensemble-mean response.

reduced in the cold tongue (Fig. 7b). An increase in near-surface stratification is diagnosed by computing the multimodel ensemble-mean vertical temperature gradient integrated over the upper 75 m (Fig. 14). A simple scaling argument indicates that in the presence of a $\overline{w} = 1$ m day^{-1} upwelling field, an anomalous thermal stratification of $\Delta T = 0.5$ K can produce an anomalous heat transport of $\Delta Q_w = -\rho_0 c_p \overline{w} \Delta T = -20$ W m^{-2}. This shows how small changes in stratification, such as those simulated by the GCMs, can result in large ocean cooling in regions of vigorous upwelling.

The changes in Q_u and Q_w are intimately related through changes in the thermocline because we are computing the heat budget on z levels. In the cold tongue, the shoaling of the thermocline drives both a positive ΔQ_u through changes in the EUC, and a negative ΔQ_w through anomalous stratification. However, many of these changes cancel out, leaving a net cooling ΔQ_w that could be attributed to a sharper thermocline. These changes would not be explicit in isopycnal coordinates, the natural coordinate system for adiabatic changes, such as the shoaling of the thermocline. Nonetheless, z coordinates allow for a simpler computation of the heat budget from the CMIP3 data. Further details on the interaction of upwelling, the EUC, and the thermocline changes are given in the appendix.

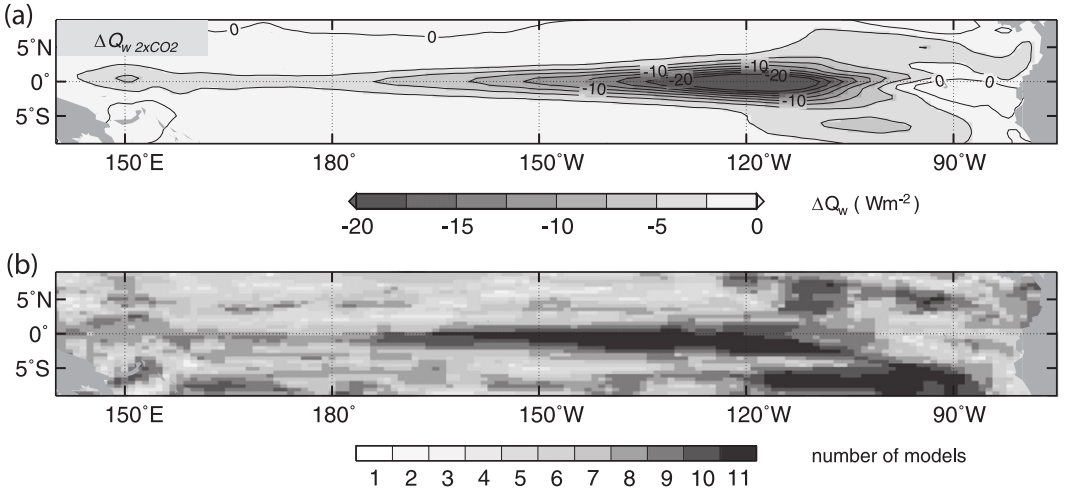

FIG. 13. (a) Multimodel ensemble-mean changes in vertical ocean heat transport in response to $2 \times CO_2$. Positive values imply heating of the ocean surface layer. (b) Number of models simulating a vertical ocean heat transport change with the same sign as the 11-model ensemble-mean response.

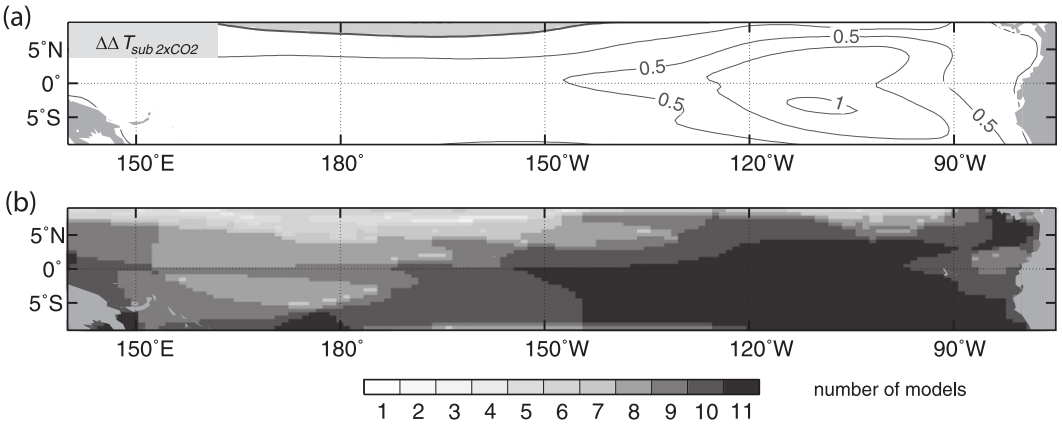

FIG. 14. (a) Multimodel ensemble-mean change in near-surface thermal stratification in response to $2 \times CO_2$. The near-surface stratification is defined as the vertically integrated vertical temperature gradient over the model layers within the upper 75 m. The contour interval is 0.25 K. (b) Number of models simulating a thermal stratification change with the same sign as the 11-model ensemble-mean response.

The heat budget is closed by computing a residual between Q_{net}, the heat storage rate Q_t, and the advective ocean heat transports, Q_u, Q_v, and Q_w. This residual accounts for ocean heat transport by subgrid-scale (SGS) ocean processes, such as vertical mixing in the surface layer and lateral mixing by ocean eddies, and submonthly variability in resolved currents. The terms of the temperature equation corresponding to these processes are not available in the CMIP3 dataset. More details on this residual and additional evidence showing the link with SGS processes are given in the appendix. The multimodel residual changes are not negligible and show a similar spatial pattern to that of ΔQ_v, but with an opposite sign (Fig. 15). The signature of the implied anomalous ocean cooling is consistent with reduced mixing associated with weaker meridional SST gradients. The multimodel response is not robust and is dominated by those models that simulate a larger equatorial warming.

9. Transient stratification response

Processes outside the equatorial Pacific could also influence the anomalous thermal stratification in response to $2 \times CO_2$. Observational and model studies indicate that the equatorial thermocline is fed by waters subducted in the eastern subtropics through distinct pathways involving the Equatorial Undercurrent (EUC) and subtropical cells (Liu et al. 1994; Lu and McCreary 1995). If SSTs were to change uniformly over the Pacific Ocean, the equatorial thermocline temperature would ultimately be modified by water subducted in the subtropics, potentially damping the anomalous equatorial stratification on gyre-adjustment time scales. However, a permanent anomalous equatorial stratification could also result from the different GW responses between the equatorial and the subtropical oceans (Seager and Murtugudde 1997; Liu 1998). The SST response simulated by the IPCC AR4/CMIP3 models shows a marked meridional contrast with enhanced warming at the equator (Liu et al. 2005). This is consistent with previous observational and modeling studies, indicating smaller subtropical SST sensitivities linked with larger wind speeds and low relative humidity (e.g., Seager et al. 2003).

In this context, we analyze the transient and equilibrium response of the multimodel near-surface thermal stratification throughout the full length of the $2 \times CO_2$ experiments (years 1–200). The Niño-3 near-surface thermal stratification, defined as the temperature between the surface and at 75-m depth,[1] increases in all models during the transient climate response and remains constant at about 0.5 K after year 71, when CO_2 is doubled and held constant (Fig. 16). This result is consistent with the relatively simpler GCM experiments (Seager and Murtugudde 1997) and box-model analysis (Liu 1998), suggesting that the stratification response in the cold tongue is a permanent feature of the equilibrium $2 \times CO_2$ climate ultimately controlled by the response of the subtropics to GW. Nonetheless, our analysis shows that the ensemble-mean stratification response follows the CO_2 curve at lags that may be too short compared with the decadal time scales typical of the adjustment of the equatorial thermocline to changes in the subtropics. Whether the equilibrium stratification

[1] This definition of stratification is equivalent to the vertically integrated vertical temperature gradient: $\int_{-H}^{0} \partial T/\partial z \, dz = T(0) - T(-H)$. Thus, the changes in SST minus T_{75m} (Fig. 16) are equivalent to the changes in vertically integrated $\partial T/\partial z$ (Fig. 14).

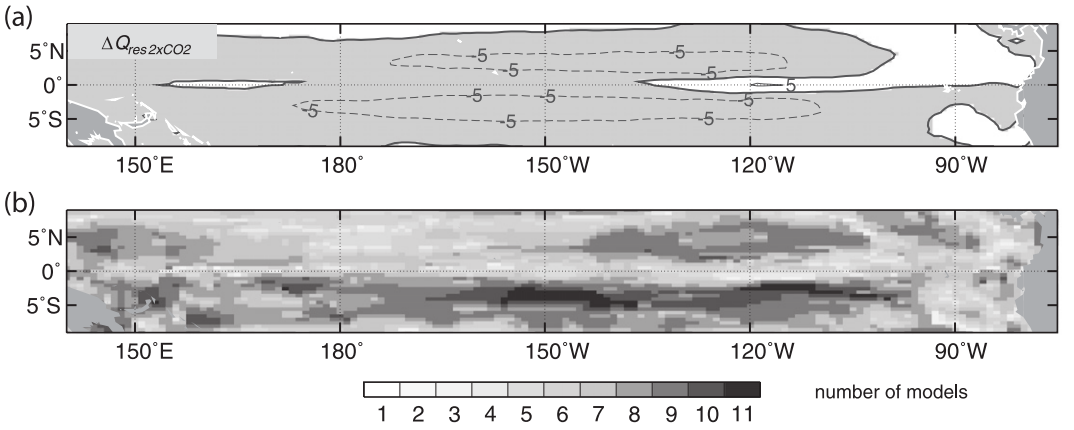

FIG. 15. (a) Multimodel ensemble-mean changes in ocean heat transport residual in response to $2 \times CO_2$. Positive values indicate heating of the ocean surface layer. The contour interval is 5 W m^{-2}. Grayed regions and dashed contours indicate negative values. (b) Number of models simulating a positive $2 \times CO_2$ change in ocean heat transport residual having the same sign as the ensemble-mean response.

response is driven from the subtropics or results from a dynamical/thermodynamical response within the equatorial Pacific remains unclear from this analysis and will be addressed in a separate study devoted to the thermocline response.

10. Discussion and conclusions

This heat budget analysis shows that in 11 state-of-the-art coupled GCMs, the climate response of the equatorial Pacific to doubling of CO_2 concentrations is determined by the superposition of the ocean dynamical response to a weaker Walker circulation and enhanced ocean cooling driven by increased near-surface thermal stratification. Weaker zonal ocean currents driven by a slowing down of the Walker circulation reduce the ocean lateral heat flux divergence throughout the basin. This ocean dynamical heating is superposed onto the $2 \times CO_2$ clear-sky radiation response, enhancing the surface warming. In the warm pool, this radiative plus ocean dynamical warming is balanced by evaporation and cloud feedbacks. In contrast, over the cold tongue, this total heating is balanced by increased ocean vertical heat transport. This ocean dynamical cooling is the sole cooling term in the heat budget changes of the cold tongue and results from increased near-surface thermal stratification in spite of a reduction in vertical velocity.

The spatial pattern of the multimodel ocean response depends on the following features of the control climate: 1) the location of upwelling in the cold tongue, 2) the

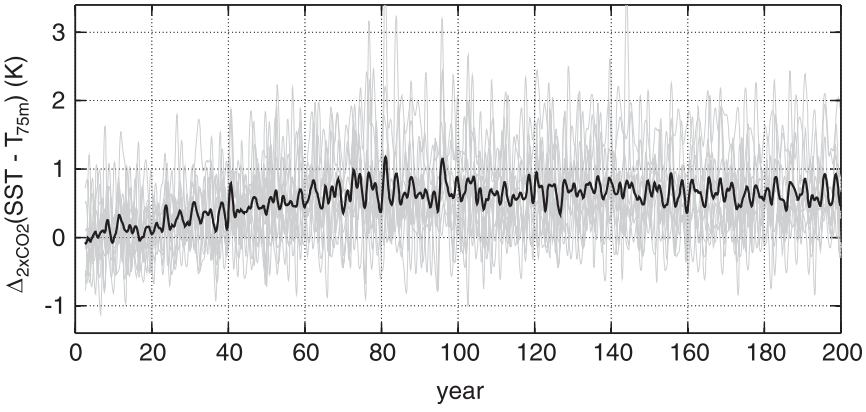

FIG. 16. Transient and equilibrium $2 \times CO_2$ response of the multimodel ensemble-mean near-surface thermal stratification over the Niño-3 region (solid black line). The near-surface stratification is defined as the vertically integrated vertical temperature gradient over the model layers within the upper 75 m. This definition is equivalent to the difference between the sea surface temperature and the temperature at 75 m. The time series of each individual model are shown in gray.

location of the zonal SST gradient, that is, the edge of the warm pool, and 3) the outcropping of the EUC. In current-generation IPCC class models these features of the mean climate extend excessively westward compared with observations associated with a well-known ''cold tongue bias.'' This bias is much smaller in MRI CGCM2.3.2, which is flux corrected. In this model, the changes in oceanic heat divergence are similar to the ensemble mean; however, they are shifted to the east following the location of the edge of the warm pool and the cold tongue. On the other hand, INM-CM3.0 simulates a cold tongue extending throughout the entire basin. The absence of a strong zonal SST gradient results in a negligible ocean dynamical heating driven by weaker surface currents. In general, the intermodel spread in the heat budget responses is as large as the multimodel mean, despite robust changes in the sign of the response. This spread is likely to result from differences in the mean climate in the individual models, for example, zonal SST gradient and upwelling, rather from the changes in currents or stratification.

Vertical heat transport provides an efficient mechanism for limiting the SST response in the cold tongue. For instance, the multimodel SST increase of about 2 K is associated with a larger stabilizing response by vertical ocean transport compared with cloud feedbacks or evaporative cooling. In the original Clement et al. (1996) ocean thermostat, the Bjerknes feedback was invoked in addition to increased cooling through vertical transport to explain the La Niña–like response to uniform surface heating. The difference here is that the IPCC AR4/CMIP3 models actually show nonuniform atmospheric damping, resulting from clouds and evaporation. More importantly, the models analyzed here simulate weakened trade winds, which prevent the Bjerknes feedback from amplifying the equatorial cooling, and thus the climate does not evolve into a La Niña–like state.

The balance among the different processes is a robust feature of the 11 models analyzed here. While the simulated climate response involves parameterized physics, for example, clouds, ocean mixing, and atmospheric convection, the main processes governing the climate response are robust: 1) increased ocean thermal stratification in the cold tongue as originally envisioned by Clement et al. (1996); and 2) weaker ocean currents and atmospheric feedbacks stabilizing the total radiative plus ocean dynamical heating in the warm pool. The amplitude of the SST response in each model will be determined by the strength of the myriad radiative and thermodynamic feedbacks involved, however, with an important role for the evaporation and cloud feedbacks over the warm pool and the thermal stratification increase in the cold tongue. Further study is required to constrain the magnitude of these feedbacks in the GCMs.

The simulated changes in SST and SW radiation over the western equatorial Pacific are consistent with the high cloud thermostat of Ramanathan and Collins (1991). It should be noted that the stabilizing effect of high clouds has been disputed in several papers (Wallace 1992; Hartmann and Michelsen 1993; Pierrehumbert 1995). Those studies show that because the TOA SW and LW forcing of these clouds cancel, they cannot affect the planetary energy budget. However, a local version of the mechanism has not been ruled out (Waliser 1996; Sobel 2003), and could explain the models response. Whether the SW cloud feedback or evaporation feedback dominates the response of the real Pacific warm pool at high SSTs is also a matter of controversy (e.g., Graham and Barnett 1987; Ramanathan and Collins 1991; Collins et al. 1996; Wallace 1992). The simulated changes show a stronger role for cloud feedbacks (Fig. 3), resulting in an eastward expansion of the warm pool.

Moreover, according to the mechanism proposed by Vecchi and Soden (2007a), the weakening of the Walker circulation depends on the sensitivity of global-mean precipitation to GW. While a sensitivity of global-mean precipitation about 2% K^{-1} is a robust feature of IPCC class GCMs, it is unclear whether GCMs underestimate it compared with observations (Wentz et al. 2007; Lambert et al. 2008). According to our results, better understanding of this sensitivity will improve the projections of the changes in the trade winds in response to increased GHGs and of equatorial SSTs as a result.

The results of this study have additional implications for ongoing efforts to detect the response of the tropical Pacific to GHG forcing. For instance, observational datasets do not agree on the SST trends in the equatorial Pacific (Vecchi et al. 2008; Karnauskas et al. 2009). This ensemble of models suggests that the detection of the $2 \times CO_2$ response may be clearer in the depth of the thermocline, not necessarily correlated with sea level on GW time scales or sea level pressure, rather than in SST. Moreover, the simulated response to $2 \times CO_2$ suggests that the apparent inconsistency between the observed changes in SST and SLP gradients may be physical; that is, a reduction in zonal SLP gradient can occur even if the zonal SST gradient is not significantly altered. This is physically consistent with the mechanism proposed by Vecchi and Soden (2007a) in which the weakening of the Walker circulation results from global constraints on the hydrologic cycle, rather than from the coupled equatorial climate. The results presented here also point to mechanisms that may be detectable with current observational networks. For example, the key processes in the ocean response—reduced zonal currents and increased stratification—may be detectable in the future when observations from the TAO array become

long enough to isolate the GW trends from the strong Pacific interannual variability.

Acknowledgments. We acknowledge the various international modeling groups participating in IPCC AR4, the Program for Climate Model Diagnosis and Intercomparison (PCMDI), and the IPCC Data Archive at Lawrence Livermore National Laboratory (supported by the Office of Science, U.S. Department of Energy) for providing the data that made this analysis possible. This research was carried out in part under the auspices of the Cooperative Institute for Marine and Atmospheric Studies (CIMAS), a Joint Institute of the University of Miami and the National Oceanic and Atmospheric Administration (NOAA), Cooperative Agreement NA17 RJ1226. P. N. DiNezio and A. Clement were partially supported by NSF (Grant 0500275) and NOAA (Grant NA0604310142). We are grateful to Henk Dijkstra, Axel Timmermann, and Mark Cane for their invaluable insight along different stages of this study. The comments of three anonymous reviewers are greatly appreciated. We also thank Jay Harris and Gary Strand for their steadfast technical support.

APPENDIX

Heat Budget Changes in Fully Coupled Ocean Models

In z-level ocean general circulation models (GCMs), the conservation of heat is represented by the temperature equation,

$$\frac{\partial T}{\partial t} + \nabla \cdot (\mathbf{u}T + F_{\mathrm{SGS}}) = \frac{1}{\rho_0 c_p}\frac{\partial Q}{\partial z}, \tag{A1}$$

where $\partial T/\partial t$ is the temperature tendency, $\nabla \cdot (\mathbf{u}T + F_{\mathrm{SGS}})$ is the temperature divergence resulting from both advection by ocean currents and subgrid-scale processes (SGS), $\partial Q/\partial z$ is a heating profile representing sources and sinks of heat (e.g., atmospheric fluxes), and $\rho_0 c_p = 4.1\ 10^6\ \mathrm{J\ m^{-3}\ K^{-1}}$ is the ocean density times the specific heat of seawater.

A heat budget can be computed by vertically integrating the temperature equation over a layer of constant depth H,

$$\int_{-H}^{\eta}\frac{\partial T}{\partial t}\,dz + \int_{-H}^{\eta}\nabla\cdot(\mathbf{u}T)\,dz + \int_{-H}^{\eta}\nabla\cdot\mathbf{F}_{\mathrm{SGS}}\,dz = \frac{1}{\rho_0 c_p}(Q_{\mathrm{net}} - Q_{\mathrm{SWpen}}), \tag{A2}$$

where the net surface heat flux Q_{net} enters the right-hand side as $Q_{\mathrm{net}}/\rho_0 c_p H$ and Q_{SWpen} is shortwave radiation that penetrates into the surface layer and leaves at its base. The flux Q_{SWpen} can be neglected if H is sufficiently deep.

The resulting heat budget can expressed as

$$\frac{\partial Q}{\partial t} = Q_{\mathrm{net}} + Q_u + Q_v + Q_w + Q_{\mathrm{SGS}}, \tag{A3}$$

where Q_t is the vertically integrated heat storage rate

$$\rho_0 c_p \frac{\partial}{\partial t}\int_{-H}^{0} T\,dz, \tag{A4}$$

and the ocean heat flux divergence resulting from resolved currents are

$$\begin{aligned} Q_u &= -\rho_0 c_p \int_{-H}^{0} u\frac{\partial T}{\partial x}\,dz \\ Q_v &= -\rho_0 c_p \int_{-H}^{0} v\frac{\partial T}{\partial y}\,dz \\ Q_w &= -\rho_0 c_p \int_{-H}^{0} w\frac{\partial T}{\partial z}\,dz, \end{aligned} \tag{A5}$$

and Q_{SGS} is the ocean heat transport by unresolved processes. In equilibrium, the long-term temperature tendency is negligible and so is the heat storage rate Q_t. The heat budget is thus balanced by the surface heat flux Q_{net} and the oceanic heat convergence by ocean currents Q_u, Q_v, and Q_w, and by ocean SGS processes Q_{SGS}.

The spatial derivatives in (A5) are computed as centered differences, instead of using the computational grid of the individual models, because some model variables are interpolated into regular grids in the CMIP3 dataset. The advective part of the divergence operator $\mathbf{u}\cdot\nabla T$ is used instead of $\nabla\cdot(\mathbf{u}T)$, the full divergence operator. Finite-volume discretization schemes use this operator to enforce the conservation laws during the numerical integration. Nonetheless, its use is not critical when diagnosing processes from model output. Achieving an exact balance of the heat budget is not possible using the CMIP3 dataset for additional reasons. For instance, high-frequency correlations between the temperature gradients and the velocity fields are not available in the CMIP3 dataset, because the variables are archived as monthly means separately. These high-frequency correlations could be important in the equatorial ocean where the eddy heat transport resulting from tropical instability waves (TIWs) is important both in high-resolution

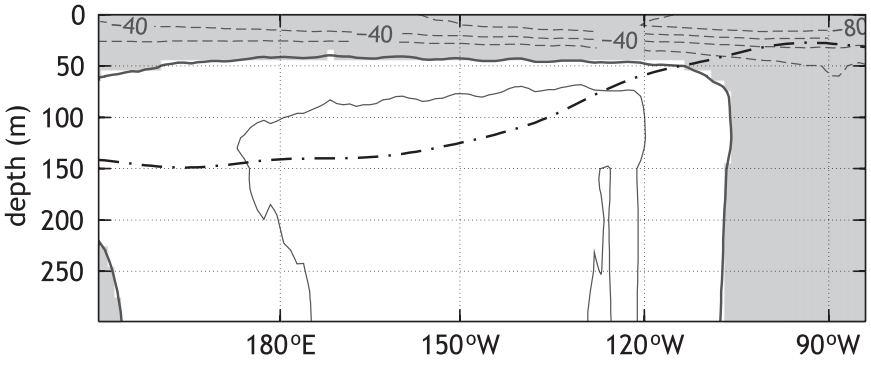

FIG. A1. (a) Multimodel ensemble-mean ocean heat transport residual in the control experiments as a function of depth of integration and longitude. Positive values indicate heating of the ocean surface layer. The contour interval is 20 W m^{-2}. Grayed regions and dashed contours indicate negative values. The depth dependent heat transport residual are averaged over an equatorial band between 2°S and 2°N. The dashed–dotted line indicates the location of the ensemble-mean maximum vertical temperature gradient in the control climate, that is, the thermocline.

ocean models (Jayne and Marotzke 2002) and observations (Stammer 1997). However, current-generation ocean climate models simulate these waves and other mesoscale phenomena poorly (Wittenberg et al. 2006); therefore, using monthly fields is expected to represent a minor discrepancy.

Ideally all of the SGS terms in the temperature equation solved by GCMs should be analyzed to close the heat budget (A3) and therefore diagnose all changes in ocean heat divergence. However, this is not possible with the CMIP3 dataset because the terms in (A1) corresponding to SGS processes are not archived. However, the ocean heat transport by SGS processes and submonthly resolved ocean dynamics can be inferred from a residual

$$Q_{\text{res}} = Q_t - Q_{\text{net}} - (Q_u + Q_v + Q_w). \qquad \text{(A6)}$$

A positive residual term Q_{res} represents a heating tendency for the heat storage rate Q_t, and thus for the vertically averaged temperature over a given constant depth layer. The depth dependence of this residual can be explored by computing Q_{res} using (A6), when the advection terms (A5) and the heat storage rate (A4) are integrated from the surface to the different model depths. The depth dependence of this residual strongly suggests a link with SGSs processes (Fig. A1). For instance, negative Q_{res} values are obtained if the heat budget (A2) is integrated within the upper 50 m. This indicates that additional cooling is needed at the base of the surface layer to balance advection and surface heat fluxes. This is consistent with SGS processes, such as vertical mixing resulting from parameterized wind stirring and entrainment. The residual heating below the mixed layer could be related to lateral mixing resulting from parameterized ocean eddies. The absence of changes in the residual below for integration depths below the thermocline suggests no heating sources/sinks consistent with a nearly adiabatic interior.

Sensitivity of the heat budget changes to the depth of integration

Estimating the ocean heat flux divergence on a constant depth layer (A5), while being physically consistent, poses limitations to fully describing the influence of some of the ocean processes in the heat budget of the ocean mixed layer. For instance, this is important for characterizing the changes involving the thermocline, which intersects constant depth surfaces. For instance, the shoaling of the thermocline not only drives anomalous stratification within the upper 75 m of the ocean in the east (Fig. 14), but also anomalous subsurface eastward currents associated with a shallower EUC. These anomalous zonal currents drive the anomalous ocean dynamical heating ΔQ_u in the cold tongue (Fig. 11a).

The depth dependence of the ocean advection terms in the heat budget can also be analyzed by integrating (A5) from the surface to the different layers in the ocean model. An equatorial section of the depth-dependent changes in Q_u show anomalous ocean dynamical heating driven both by a weakening of surface zonal currents in the west and by a shallower EUC that outcrops further west in the 2 × CO_2 climate (Fig. A2a). Note that the panels in Fig. A2 show the sensitivity of the advection terms (A5) to different depths of integration and are not

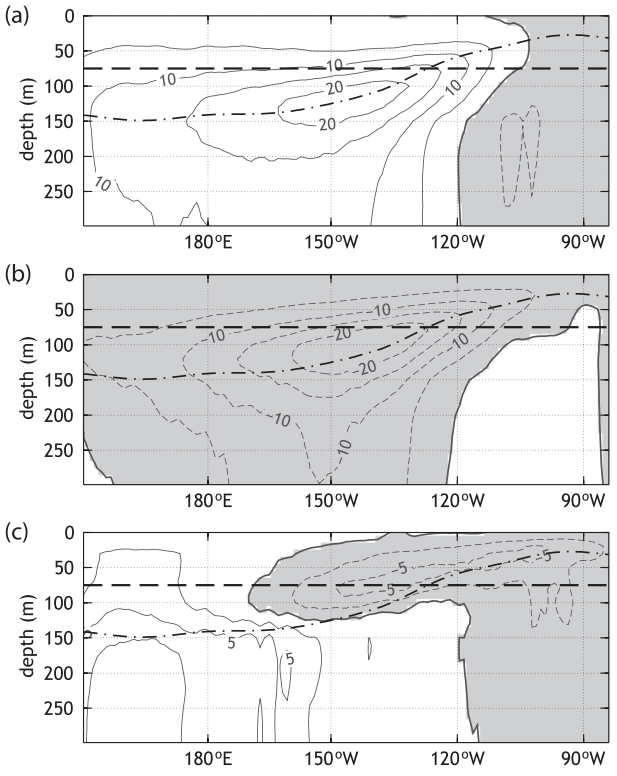

FIG. A2. Multimodel ensemble-mean changes in (a) zonal, (b) vertical, and (c) zonal plus vertical ocean heat transport in response to 2 × CO_2. The equatorial sections show the zonal and vertical advection terms in the heat budget equation as function of the depth of integration. Positive values indicate heating of the ocean surface layer. The contour interval is 5 W m^{-2} in (a) and (b), and 2.5 W m^{-2} in (c). Grayed regions and dashed contours indicate negative values. The dashed line delimits the 75-m-depth slab corresponding to the heat transport changes presented in this study. In both panels, the changes are averaged over an equatorial band between 5°S and 5°N. The dashed–dotted line indicates the location of the maximum vertical temperature gradient in the control climate, that is, the thermocline.

the integrands in (A2). Thus, net heating is indicated where the plotted values increase with H, rather than where they are positive.

The anomalous surface and subsurface heating driven by a shallower EUC is compensated by changes in vertical heat transport also associated with a shallower thermocline (Fig. A2b). The net $Q_u + Q_w$ changes (Fig. A2c) show net heating in the west and net cooling in the east if the heat budget is integrated over depths within the mixed layer. In the west the heating is limited to the upper 50 m where *surface* currents weaken in response to the winds. In the east, the net cooling changes are located in the base of the mixed layer above the thermocline, suggesting a strong role for anomalous vertical heat transport driven by a sharper thermocline.

REFERENCES

Bjerknes, J., 1969: Atmospheric teleconnections from the equatorial Pacific. *Mon. Wea. Rev.,* **97,** 163–172.

Bunge, L., and A. J. Clarke, 2009: A verified estimation of the El Niño index Niño-3.4 since 1877. *J. Climate,* **22,** 3979–3992.

Cane, M. A., 1979: The response of an equatorial ocean to simple wind stress patterns. I: Model formulation and analytic results. *J. Mar. Res.,* **37,** 233–252.

——, A. C. Clement, A. Kaplan, Y. Kushnir, D. Pozdnyakov, R. Seager, S. E. Zebiak, and R. Murtugudde, 1997: Twentieth century sea surface temperature trends. *Science,* **275,** 957–960.

Clement, A. C., R. Seager, M. A. Cane, and S. E. Zebiak, 1996: An ocean dynamical thermostat. *J. Climate,* **9,** 2190–2196.

Collins, M., CMIP Modeling Groups, 2005: El Nino- or La Nina-like climate change? *Climate Dyn.,* **24,** 89–104.

Collins, W. D., F. P. J. Valero, P. J. Flatau, D. Lubin, H. Grassl, P. Pilewskie, and J. Spinherne, 1996: Radiative effects of convection in the tropical Pacific. *J. Geophys. Res.,* **101,** 14 999–15 012.

——, and Coauthors, 2006: The Community Climate System Model version 3 (CCSM3). *J. Climate,* **19,** 2122–2143.

Cubasch, U., and Coauthors, 2001: Projections of future climate change. *Climate Change 2001: The Scientific Basis,* J. T. Houghton et al., Eds., Cambridge University Press, 527–582.

Delworth, T. L., and Coauthors, 2006: GFDLs CM2 global coupled climate models. Part I: Formulation and simulation characteristics. *J. Climate,* **19,** 643–674.

Dijkstra, H. A., and J. D. Neelin, 1995: Ocean–atmosphere interaction and the tropical climatology. Part II: Why the Pacific cold tongue is in the east. *J. Climate,* **8,** 1343.

Fedorov, A. V., and S. G. Philander, 2000: Is El Niño changing? *Science,* **288,** 1997–2002.

——, and ——, 2001: A stability analysis of tropical ocean–atmosphere interactions: Bridging measurements and theory for El Niño. *J. Climate,* **14,** 3086–3101.

Flato, G. M., and G. J. Boer, 2001: Warming asymmetry in climate change simulations. *Geophys. Res. Lett.,* **28,** 195–198.

Gnanadesikan, A., J. L. Russell, and F. Zeng, 2007: How does ocean ventilation change under global warming? *Ocean Sci.,* **3,** 43–53.

Goosse, H., and T. Fichefet, 1999: Importance of ice-ocean interactions for the global ocean circulation: A model study. *J. Geophys. Res.,* **104,** 337–355.

Graham, N. E., and T. P. Barnett, 1987: Sea surface temperature, surface wind divergence, and convection over the tropical oceans. *Science,* **238,** 657–659.

Hansen, J., and Coauthors, 2005: Earth's energy imbalance: Confirmation and implications. *Science,* **308,** 1431–1435, doi:10.1126/science.1110252.

——, M. Sato, R. Ruedy, K. Lo, D. W. Lea, and M. Medina-Elizade, 2006: Global temperature change. *Proc. Natl. Acad. Sci. USA,* **103,** 14 288–14 293.

Hartmann, D. L., and M. L. Michelsen, 1993: Large-scale effects on the regulation of tropical sea surface temperature. *J. Climate,* **6,** 2049–2062.

Hasumi, H., and S. Emori, Eds., 2004: K-1 coupled model (MIROC) description. Center for Climate System Research, University of Tokyo, K-1 Tech. Rep. 1, 34 pp.

Held, I. M., and B. J. Soden, 2006: Robust responses of the hydrological cycle to global warming. *J. Climate,* **19,** 5686–5699.

Hoerling, M., and A. Kumar, 2003: The perfect ocean for drought. *Science,* **299,** 691–694.

Jayne, S. R., and J. Marotzke, 2002: The oceanic eddy heat transport. *J. Phys. Oceanogr.,* **32,** 3328–3345.

Jin, F.-F., 1996: Tropical ocean-atmosphere interaction, the Pacific cold-tongue, and the El Niño-Southern Oscillation. *Science,* **274,** 76–78.

Karnauskas, K., R. Seager, A. Kaplan, Y. Kushnir, and M. Cane, 2009: Observed strengthening of the zonal sea surface temperature gradient across the equatorial Pacific Ocean. *J. Climate,* **22,** 4316–4321.

Klein, S. A., and D. L. Hartmann, 1993: The seasonal cycle of low stratiform clouds. *J. Climate,* **6,** 1587–1606.

Knutson, T. R., and S. Manabe, 1995: Time-mean response over the tropical Pacific to increased CO_2 in a coupled ocean–atmosphere model. *J. Climate,* **8,** 2181–2199.

Lambert, F. H., A. R. Stine, N. Y. Krakauer, and J. C. H. Chiang, 2008: How much will precipitation increase with global warming? *Eos, Trans. Amer. Geophys. Union,* **89,** doi:10.1029/2008EO210001.

Liu, Z., 1998: The role of the ocean in the response of tropical climatology to global warming: The west–east SST contrast. *J. Climate,* **11,** 864–875.

——, S. G. H. Philander, and R. C. Pacanowski, 1994: A GCM study of tropical–subtropical upper-ocean water exchange. *J. Phys. Oceanogr.,* **24,** 2606–2623.

——, S. J. Vavrus, F. He, N. Wen, and Y. Zhang, 2005: Rethinking tropical ocean response to global warming: The enhanced equatorial warming. *J. Climate,* **18,** 4684–4700.

Lu, P., and J. P. McCreary, 1995: Influence of the ITCZ on the flow of thermocline water from the subtropical to the equatorial ocean. *J. Phys. Oceanogr.,* **25,** 3076–3088.

Marsland, S. J., H. Haak, J. H. Jungclaus, M. Latif, and F. Roeske, 2003: The Max-Planck-Institute global ocean/sea ice model with orthogonal curvilinear coordinates. *Ocean Modell.,* **5,** 91–127.

McPhaden, M. J., 1993: TOGA-TAO and the 1991–93 El Niño-Southern Oscillation event. *Oceanography,* **6,** 36–44.

——, and D. Zhang, 2002: Slowdown of the meridional overturning circulation in the upper Pacific Ocean. *Nature,* **415,** 603–608.

Meehl, G. A., and W. M. Washington, 1996: El Niño-like climate change in a model with increased atmospheric CO_2 concentrations. *Nature,* **382,** 56–60.

——, W. D. Collins, B. A. Boville, J. T. Kiehl, T. M. L. Wigley, and J. M. Arblaster, 2000: Response of the NCAR Climate System Model to increased CO_2 and the role of physical processes. *J. Climate,* **13,** 1879–1898.

——, and Coauthors, 2007: Global climate projections. *Climate Change 2007: The Physical Science Basis*, S. Solomon et al., Eds., Cambridge University Press, 747–845.

Philander, S. G. H., 1981: The response of equatorial oceans to a relaxation of the trade winds. *J. Phys. Oceanogr.,* **11,** 176–189.

Pierrehumbert, R. T., 1995: Thermostats, radiator fins, and the local runaway greenhouse. *J. Atmos. Sci.,* **52,** 1784–1806.

Ramanathan, V., and W. Collins, 1991: Thermodynamic regulation of ocean warming by cirrus clouds deduced from observations of the 1987 El Niño. *Nature,* **351,** 27–32.

Salas-Mélia, D., and Coauthors, 2005: Description and validation of the CNRM-CM3 global coupled model. CNRM Working Note 103, 36 pp.

Schubert, S. D., 2004: On the cause of the 1930s Dust Bowl. *Science,* **303,** 1855–1859.

Seager, R., and R. Murtugudde, 1997: Ocean dynamics, thermocline adjustment and regulation of tropical SST. *J. Climate,* **10,** 521–539.

——, S. E. Zebiak, and M. A. Cane, 1988: A model of the tropical Pacific sea-surface temperature climatology. *J. Geophys. Res.,* **93** (C2), 1265–1280.

——, R. Murtugudde, A. Clement, and C. Herweijer, 2003: Why is there an evaporation minimum at the equator? *J. Climate,* **16,** 3793–3802.

——, Y. Kushnir, C. Herweijer, N. Naik, and J. Velez, 2005: Modeling of tropical forcing of persistent droughts and pluvials over western North America: 1856–2000. *J. Climate,* **18,** 4065–4088.

Sobel, A. H., 2003: On the coexistence of an evaporation minimum and precipitation maximum in the warm pool. *J. Climate,* **16,** 1003–1009.

Soden, B. J., and I. M. Held, 2006: An assessment of climate feedbacks in coupled ocean–atmosphere models. *J. Climate,* **19,** 3354–3360.

Stammer, D., 1997: Global characteristics of ocean variability from regional TOPEX/Poseidon altimeter measurements. *J. Phys. Oceanogr.,* **27,** 1743–1769.

Takahashi, K., 2009: The global hydrological cycle and atmospheric shortwave absorption in climate models under CO_2 forcing. *J. Climate,* in press.

Timmermann, A., J. Oberhuber, A. Bacher, M. Esch, M. Latif, and E. Roeckner, 1999: Increased El Niño frequency in a climate model forced by future greenhouse warming. *Nature,* **398,** 694–696.

Vecchi, G. A., and B. J. Soden, 2007a: Global warming and the weakening of the tropical circulation. *J. Climate,* **20,** 4316–4340.

——, and ——, 2007b: Effect of remote sea surface temperature change on tropical cyclone potential intensity. *Nature,* **450,** 1066–1070, doi:10.1038/nature06423.

——, ——, A. T. Wittenberg, I. M. Held, A. Leetmaa, and M. J. Harrison, 2006: Weakening of tropical Pacific atmospheric circulation due to anthropogenic forcing. *Nature,* **441,** 73–76, doi:10.1038/nature04744.

——, A. Clement, and B. J. Soden, 2008: Examining the tropical Pacific's response to global warming. *Eos, Trans. Amer. Geophys. Union,* **89,** doi:10.1029/2008EO090002.

Volodin, E. M., and N. A. Diansky, 2004: El Niño reproduction in coupled general circulation model. *Russ. Meteor. Hydrol.,* **12,** 5–14.

Waliser, D. E., 1996: Formation and limiting mechanisms for very high sea surface temperature: Linking the dynamics and the thermodynamics. *J. Climate,* **9,** 161–188.

Wallace, J., 1992: Effect of deep convection on the regulation of tropical sea surface temperature. *Nature,* **357,** 230–231.

Wang, C., and S.-K. Lee, 2008: Global warming and United States landfalling hurricanes. *J. Geophys. Res.,* **35,** L02708, doi:10.1029/2007GL032396.

Wentz, F. J., L. Ricciardulli, K. Hilburn, and C. Mears, 2007: How much more rain will global warming bring? *Science,* **317,** 233–235.

Wittenberg, A. T., A. Rosati, N.-C. Lau, and J. J. Ploshay, 2006: GFDL's CM2 global coupled climate models. Part III: Tropical Pacific climate and ENSO. *J. Climate,* **19,** 698–722.

Wyrtki, K., 1981: An estimate of equatorial upwelling in the Pacific. *J. Phys. Oceanogr.,* **11,** 1205–1214.

Yu, Y. Q., X. H. Zhang, and Y. F. Guo, 2004: Global coupled ocean-atmosphere general circulation models in LASG/IAP. *Adv. Atmos. Sci.,* **21,** 444–455.

Yukimoto, S., and A. Noda, 2002: Improvements in the Meteorological Research Institute Global Ocean-Atmosphere Coupled GCM (MRI-CGCM2) and its climate sensitivity. NIES Tech. Rep. 10, 8 pp.

Zhang, M., and H. Song, 2006: Evidence of deceleration of atmospheric vertical overturning circulation over the tropical Pacific. *Geophys. Res. Lett.,* **33,** L12701, doi:10.1029/2006GL025942.